

## Phase coexistence in melting aluminum clusters

Baopeng Cao, Anne K. Starace, Oscar H. Judd, and Martin F. Jarrold<sup>a)</sup>*Department of Chemistry, Indiana University, 800 East Kirkwood Avenue,  
Bloomington, Indiana 47405, USA*

(Received 7 September 2008; accepted 15 April 2009; published online 26 May 2009)

The internal energy distributions for melting aluminum cluster cations with 100, 101, 126, and 127 atoms have been investigated using multicollision induced dissociation. The experimental results can be best fit with a statistical thermodynamic model that incorporates only fully solidlike and fully liquidlike clusters so that the internal energy distributions become bimodal during melting. This result is consistent with computer simulations of small clusters, where rapid fluctuations between entirely solidlike and entirely liquidlike states occur during the phase change. To establish a bimodal internal energy distribution, the time between the melting and freezing transitions must be longer than the time required for equilibration of the energy distribution (which is estimated to be around 1–2  $\mu\text{s}$  under our conditions). For  $\text{Al}_{100}^+$  and  $\text{Al}_{101}^+$ , the results indicate that this criterion is largely met. However, for  $\text{Al}_{126}^+$  and  $\text{Al}_{127}^+$ , it appears that the bimodal energy distributions are partly filled in, suggesting that either the time between the melting and freezing transitions is comparable to the equilibration time or that the system starts to switch to macroscopic behavior where the phase change occurs with the two phases in contact. © 2009 American Institute of Physics.

[DOI: [10.1063/1.3129525](https://doi.org/10.1063/1.3129525)]

### I. INTRODUCTION

Macroscopic objects usually melt gradually, with an almost infinite number of partially melted intermediates where the solid and liquid phases are in contact. In contrast, in computer simulations of small clusters, melting often occurs through sudden transitions between entirely solidlike and entirely liquidlike states.<sup>1–8</sup> This behavior, which is called dynamic phase coexistence, is thought to occur because of the energetic cost of the solid-liquid interface.<sup>7</sup> The cost is substantial for a small cluster but negligible for a macroscopic object where only a small fraction of the atoms is at the interface.

One signature of dynamic phase coexistence is that a canonical ensemble has a bimodal internal energy distribution during the phase change, where the low energy component is due to entirely solidlike clusters and the high energy component is due to entirely liquidlike clusters. There are rapid fluctuations between the solidlike and liquidlike states and as the ensemble melts, the fraction of liquidlike clusters increases and the fraction of solidlike clusters shows a corresponding decrease (see upper panel of Fig. 1). For static phase coexistence (which occurs with macroscopic objects), the internal energy distribution for each object has a single component that shifts over from the energy for the solid to the energy of the liquid as the solid melts (see lower panel of Fig. 1).<sup>9</sup> In this case, the energy distribution for an ensemble depends on whether or not melting is synchronized. For an ensemble of identical macroscopic objects that are all heated to slightly above their melting temperature at the same time, the energy distribution of the ensemble will be narrow and move from left to right as the objects melt. On the other

hand, if melting is unsynchronized, the energy distribution of the ensemble will be broad, extending from the energy of the solid to the energy of the liquid, and if all internal energies between fully solid and fully liquid are equally likely, the distribution will be flat topped.

According to simulations, around  $10^2$ – $10^3$  atoms are required for static phase coexistence to emerge for clusters,<sup>10–16</sup> though this has never been tested outside of a computer. It is only fairly recently that detailed experimental studies of the melting of size-selected clusters have been performed,<sup>17–24</sup> and there is not much experimental evidence to support the existence of dynamic phase coexistence. In some early work with small argon clusters, the spectral line shapes of dopant molecules were interpreted as favoring dynamic coexistence,<sup>25,26</sup> but these results are subject to other interpretations. For metal clusters, Schmidt *et al.*<sup>27</sup> reported evidence for a bimodal internal energy distribution in the melting of  $\text{Na}_{147}^+$  from measurements of the fragmentation pattern as a function of photon energy. In our studies of the melting of aluminum clusters, we found that the widths of the peaks in the heat capacities (due to the latent heats of melting) could be accounted for, in most cases, by a two state model (i.e., by considering only entirely solidlike and entirely liquidlike clusters).<sup>28,29</sup> In the work reported here we directly probe the internal energy distributions of melting aluminum cluster cations with 100, 101, 126, and 127 atoms.

It takes time to establish a bimodal internal energy distribution. The time between melting and freezing transitions must be longer than the time required for the equilibration of the clusters internal energy (which is around 1–2  $\mu\text{s}$  under our experimental conditions). So the observation of a bimodal energy distribution not only confirms the existence of dynamic phase coexistence but also places limits on the size of the rate constants for the melting and freezing transitions.

<sup>a)</sup>Electronic mail: [mjf@indiana.edu](mailto:mjf@indiana.edu).

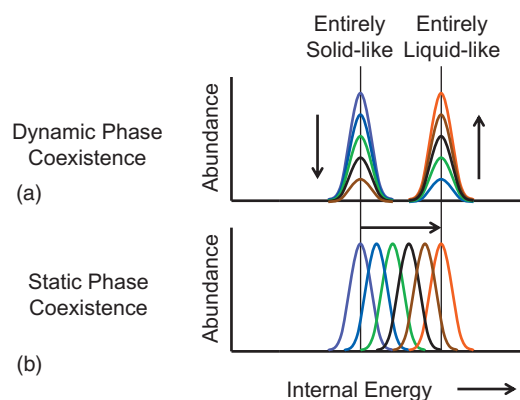


FIG. 1. (Color) Cartoon showing internal energy distributions during melting for (a) clusters showing dynamic phase coexistence and (b) a macroscopic object showing static phase coexistence. The arrows show the changes in the internal energy distribution that occur on going from solid to liquid.

Virtually nothing is known about these rates, though they are clearly relevant to understanding phase transitions in macroscopic objects.

## II. EXPERIMENTAL METHODS

The apparatus used for these studies has been described in detail elsewhere.<sup>22,29,30</sup> Briefly, aluminum clusters are generated by laser vaporization of a liquid aluminum target in a helium buffer gas. After formation, the clusters are carried through a 10 cm long temperature variable extension where their temperature is set. Clusters exit the extension through a small aperture and are focused into a quadrupole mass spectrometer where a specific cluster size is selected. The size-selected clusters are then focused into a collision cell containing 1 torr of helium. As the clusters enter the collision cell, they undergo numerous collisions with helium, each one converting a small fraction of the ions' translational energy into internal energy. If the initial translational energy is high enough, some of the clusters may be excited to the point where they dissociate. The products and undissociated clusters are drawn across the collision cell by a weak electric field and exit through a small aperture. The exiting ions are focused into a second quadrupole mass spectrometer where they are mass analyzed and then detected. The fraction of clusters that dissociate is determined from the mass spectrum.

## III. HEAT CAPACITY MEASUREMENTS

We first briefly describe the heat capacity measurements that provide melting temperatures and latent heats for the target clusters. A detailed description of the method is given elsewhere.<sup>29</sup> In what follows, the translational energies and cluster temperatures refer to their values at the entrance of the collision cell. Mass spectra are measured for six translational energies close to the value required for 50% dissociation. The translational energy for 50% dissociation (TE50%D) is then determined from a linear regression. The change in TE50%D with the temperature is proportional to the heat capacity. The proportionality constant, the fraction of the ions' translational energy that is converted into internal

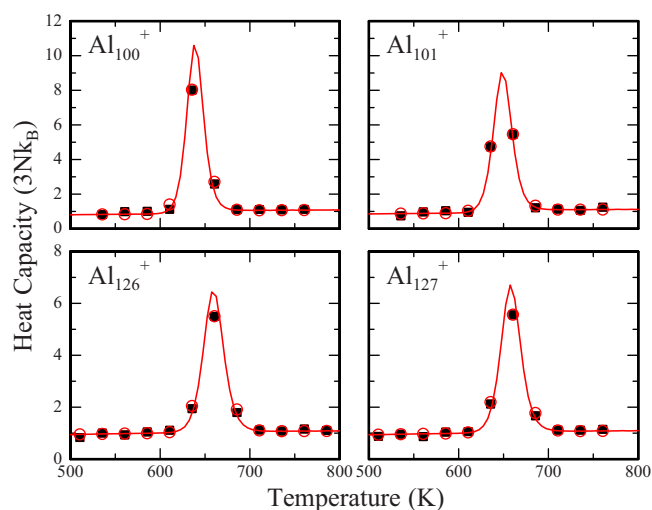


FIG. 2. (Color online) Heat capacities recorded for  $\text{Al}_{100}^+$ ,  $\text{Al}_{101}^+$ ,  $\text{Al}_{126}^+$ , and  $\text{Al}_{127}^+$ . The heat capacities are plotted in units of the classical value,  $3Nk_B$ , where  $3N = (3n - 6 + 3/2)$ . The filled squares are the experimental results (the average of three independent measurements). The unfilled circles are the results of a fit to the measurements using a two state model with  $\Delta T = 25$  K (see text). The solid line shows the calculated heat capacities for the two state model with  $\Delta T = 5$  K.

energy in collisions with helium, is obtained from an impulsive collision model.<sup>31</sup> The measurements are made with a  $\Delta T$  of 25 K.

Figure 2 shows heat capacities recorded for  $\text{Al}_{100}^+$ ,  $\text{Al}_{101}^+$ ,  $\text{Al}_{126}^+$ , and  $\text{Al}_{127}^+$ . The filled black squares are the experimental results (the average of three independent measurements). The unfilled red circles are the fit to the measurements using a two state model<sup>28,32</sup> where we assume that the liquidlike and solidlike states are in equilibrium, with an equilibrium constant given by

$$K(T) = \exp\left[-\frac{\Delta H_M}{R}\left(\frac{1}{T} - \frac{1}{T_M}\right)\right], \quad (1)$$

where  $\Delta H_M$  is the latent heat,  $R$  is the gas constant, and  $T_M$  is the melting temperature (the temperature where the number of solidlike clusters equals the number of liquidlike). The contribution of the latent heats to the heat capacity is then

$$C(T) = \frac{dE_{\text{int}}}{dT} = \frac{\Delta(-f_S(T)\Delta H_M)}{\Delta T}, \quad (2)$$

where  $f_S(T)$  is the fraction of solidlike clusters present at temperature  $T$ . Equation (2) describes the peak in the heat capacity that results from the melting transition. This calculated peak is fit to the measured peak using a least-squares procedure. More details about the fitting method are given in Ref. 28. The unfilled circles in Fig. 2 show the result of this fit with  $\Delta T = 25$  K, the same value for  $\Delta T$  as used in the experiments. The simulation fits the measured points (filled squares); however, the heat capacity peaks are very narrow. Within the framework of the two state model, this is due to the relatively large latent heats for these clusters (the larger the latent heat, the sharper the solid to liquid transition). The solid line in Fig. 2 shows the calculated heat capacity for the two state model with  $\Delta T = 5$  K. This is expected to provide a

TABLE I. Melting temperatures and latent heats determined from the least-squares fits of the two state model described in the text to the measured heat capacities.

Cluster size (Atoms)	Melting temperature (K)	Latent heat (eV)
100	640	5.96
101	649	5.53
126	660	5.17
127	658	5.27

truer representation of the shape of the heat capacity peak (because of the smaller  $\Delta T$ ).

Table I shows the melting temperatures and latent heats obtained from the least-squares fits of the two state model to the measured heat capacities (Fig. 2). The melting temperatures lie between 640 and 660 K and the latent heats are between 5 and 6 eV/cluster; both are smaller than the bulk values: 933 K and 0.1085 eV/atom (or 10.85 eV for 100 aluminum atoms).

#### IV. INTERNAL ENERGY DISTRIBUTIONS

Information about the internal energy distributions can be obtained by measuring the fraction that dissociate as a function of the clusters' translational energy. Some results for  $\text{Al}_{100}^+$  are shown in Fig. 3. The upper panel shows plots of the fraction dissociated for temperatures of 373, 620, 640, 660, and 680 K. The S-shaped thresholds shift to lower translational energy as the temperature is raised because less energy needs to be added to the hotter clusters in order to get them to dissociate. For temperatures of 600, 620, 660, and 680 K two independent, virtually overlapping data sets are plotted in Fig. 3. For 640 K (which corresponds to the center of the melting transition for  $\text{Al}_{100}^+$ ), the results of four independent measurements are shown. There is much more scatter in the results at this temperature than for the others. At the center of the melting transition, small fluctuations in the temperature lead to large changes in the amount of liquidlike and solidlike clusters present, which, in turn, lead to substantial changes in the fraction that dissociates at a given collision energy.

The lower panel in Fig. 3 shows derivatives of the fraction dissociated. A fast Fourier transform filter was used to remove the high frequency components before the derivative was taken. The derivatives appear close to Gaussian and the widths of the peaks for temperatures except for 640 K are similar. At 640 K the peak is much broader than at the other temperatures.

There are three main contributors to the widths of the derivatives. First, and perhaps the most obvious, is the internal energy distribution of the clusters. Second, a distribution of internal energies is transferred to the clusters in the multicollision excitation process that occurs in the collision cell. This distribution is expected to be narrow (and only makes a minor contribution to the width of the peak) because of averaging inherent in the multicollision excitation process.<sup>33</sup> The third contributor to the width of the peak results from the energy dependence of the dissociation rate. The dissocia-

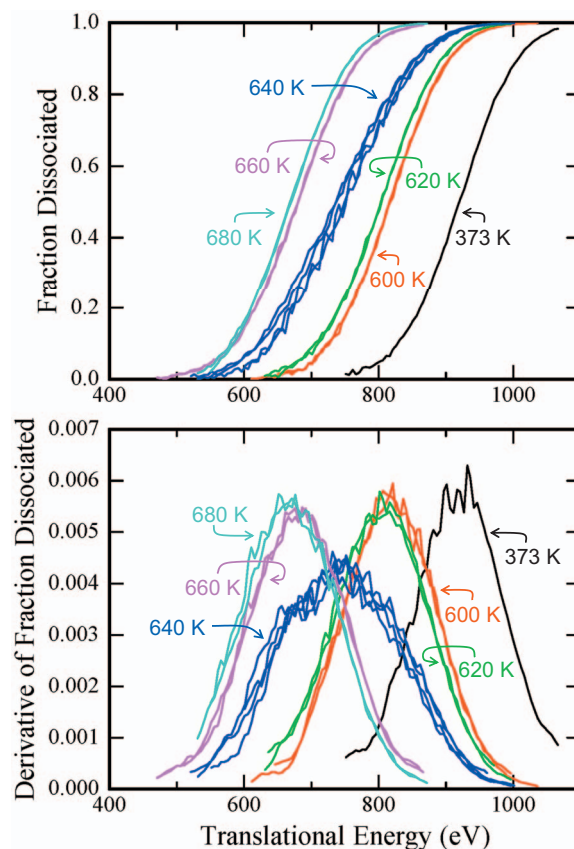


FIG. 3. (Color) The upper graph shows the fraction dissociated plotted against translational energy for  $\text{Al}_{100}^+$ . Two independent overlapping measurements are shown for temperatures of 600, 620, 660, and 680 K. Four independent measurements are shown for a temperature of 640 K (which corresponds to the center of the melting transition for  $\text{Al}_{100}^+$ ). The lower graph shows the derivative of the fraction dissociated plotted against translational energy. The fraction dissociated was smoothed with a fast Fourier transform filter to remove the high frequency components before the derivative was taken.

tion rate,  $k(E)$ , increases relatively slowly with internal energy,  $E$ , and so the fraction of clusters that dissociates on the experimental time scale,  $e^{-k(E)t}$ , increases gradually with internal energy.

The internal energy distributions for the solidlike cluster can be estimated using statistical thermodynamics. The fraction with internal energy  $E$  is given by

$$f(E, T) = \frac{\rho(E)e^{-E/k_B T}}{\int dE \rho(E)e^{-E/k_B T}}, \quad (3)$$

where  $\rho(E)$  is the density of states at energy  $E$ . We estimate  $\rho(E)$  assuming that it is dominated by the vibrations of the electronic ground state and that all  $3n-6$  oscillators have the same frequency (the Debye frequency,  $\nu$ ). Then, the number of ways of distributing  $j$  quanta among  $s$  harmonic oscillators is  $(j+s-1)!/j!(s-1)!$ , where  $j=E/h\nu$ . Around the melting temperature there are two components in the internal energy distribution, corresponding to solidlike and liquidlike. We calculate the internal energy distribution of the liquidlike clusters in the same way as the solidlike described above, but the internal energies of the liquidlike clusters are offset by the latent heat from Table I (5.96 eV for  $\text{Al}_{100}^+$ ). We assume that the solidlike and liquidlike clusters have the same Debye

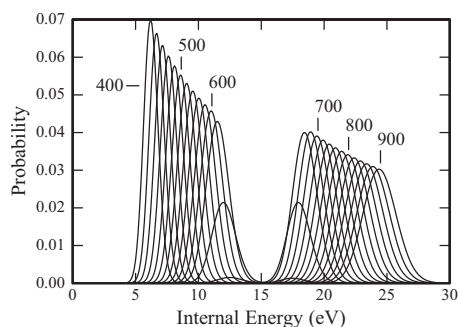


FIG. 4. Internal energy distributions calculated assuming dynamic phase coexistence (see text) for  $\text{Al}_{100}^+$  at temperatures ranging from 400 to 900 K. The center of the melting transition is at 640 K. The distributions that peak below 15 eV are due to solidlike clusters, while those that peak above 15 eV are due to liquidlike.

frequency. As noted above, we also assume that the vibrations are harmonic and that all of the cluster vibrations have the same frequency. These assumptions are significant approximations but they will not change the main features of the results. Taking into account both solidlike and the liquidlike components, the internal energy distribution is given by

$$f(E, T) = \frac{f_S(T)\rho(E)e^{-E/k_B T}}{\int dE\rho(E)e^{-E/k_B T}} + \frac{f_L(T)\rho(E - \Delta H_M)e^{-(E - \Delta H_M)/k_B T}}{\int dE\rho(E - \Delta H_M)e^{-(E - \Delta H_M)/k_B T}}, \quad (4)$$

where  $f_S(T)$  and  $f_L(T)$  are the fraction of solidlike and liquidlike clusters, respectively. These fractions are calculated assuming dynamic phase coexistence [i.e., using the equilibrium constant given in Eq. (1)]. Figure 4 shows internal energy distributions calculated using Eq. (4) for  $\text{Al}_{100}^+$  at temperatures ranging from 400 to 900 K. The distributions with internal energies less than 15 eV are solidlike clusters and those with internal energies greater than 15 eV are liquidlike.

In order to account for the widths of the peaks in the lower half of Fig. 3, it is necessary to convolute the internal energy distributions shown in Fig. 4 with functions describing the distribution of internal energies transferred in the multicollision excitation process and the fraction of clusters that dissociate on the experimental time scale as a function of the total internal energy. Instead of attempting to calculate the contributions from these two factors from scratch, we assume that they can be accounted for by a Gaussian function. We convolute the calculated internal energy distributions with the Gaussian, adjusting the width of the Gaussian to fit the 600 and 680 K peaks (i.e., the peaks that are well away from the melting transition). The results are shown in the upper half of Fig. 5 where the colored lines (with fluctuations) are the measured derivatives and the smooth black lines were obtained by convoluting the Gaussian with the calculated internal energy distributions. This approach gives a good fit to the measured peaks at 600 and 680 K using a Gaussian with the same width at both temperatures. We then calculate the distributions at 620, 640, and 660 K (where the melting transition occurs and both the liquidlike and solidlike states are involved) using the same Gaussian function. The results are shown in the upper half of Fig. 5. The plot in

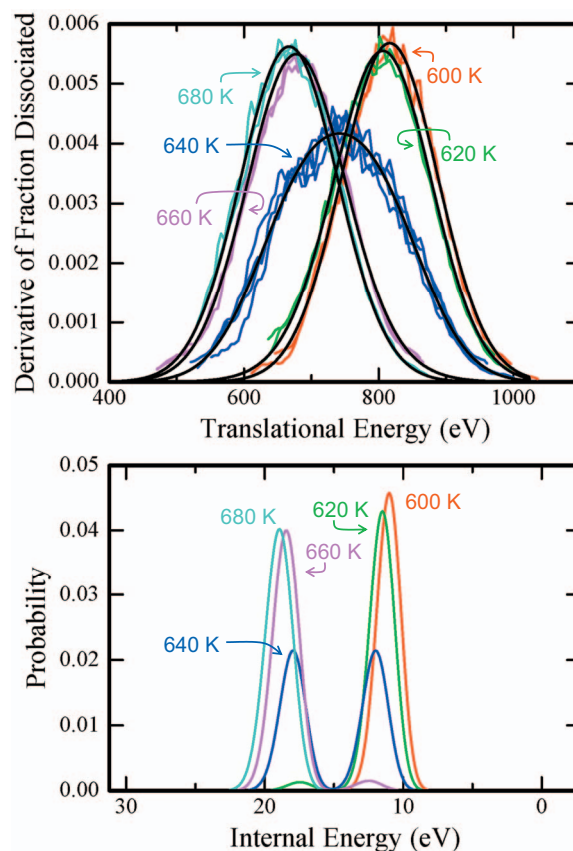


FIG. 5. (Color) The upper graph shows the derivative of the fraction dissociated plotted against translational energy for  $\text{Al}_{100}^+$  at temperatures of 600, 620, 640, 660, and 680 K. The colored lines (that show fluctuations) are the measurements from Fig. 3 and the smooth black lines are the result of simulations described in the text. The simulations use the calculated internal energy distributions shown in the lower plot. The internal energy distributions are color coded to the temperature of the plots in the upper plot.

the lower half of Fig. 5 shows the internal energy distributions used at the five temperatures in the upper half.

The simulations accurately reproduce the dramatic change in the width of the peak that occurs at the center of the melting transition (640 K). Note, however, that the broadening that results from the energy dependence of the dissociation rates and the distribution of energies transferred by multicollisional excitation (the factors accounted for by the Gaussian) obscures the bimodal nature of the internal energy distribution at the center of the melting transition.

As we have indicated above, the bimodal internal energy distribution can only be established if the time between melting and freezing transitions is larger than the time required for equilibration of the internal degrees of freedom. If melting and freezing transitions occur much more rapidly than equilibration, then the dip between the two components in the internal energy distribution will disappear. In the limit where the time between melting and freezing transitions is much shorter than the equilibration time, the bimodal distribution will be replaced by a single narrow peak. Equilibration occurs through collisions with the helium buffer gas in the extension and we can estimate its time scale by assuming that the energy is equilibrated between the colliding helium

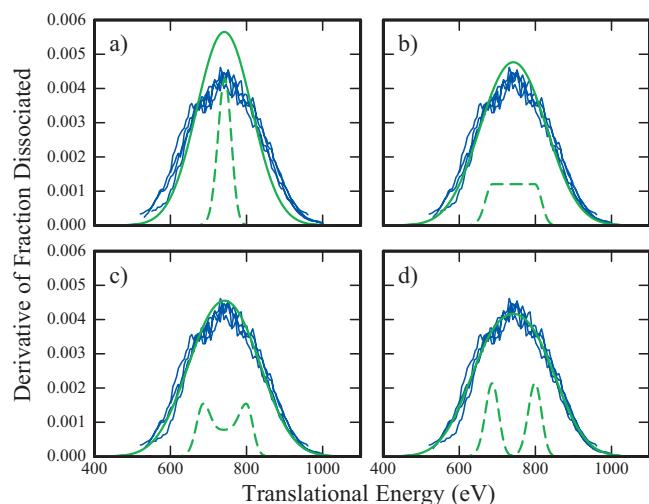


FIG. 6. (Color) Comparison of the simulation with experiment for  $\text{Al}_{100}^+$  at 640 K (the center of the melting transition) for different internal energy distributions. The dashed lines show the internal energy distributions used in the simulations offset and plotted on the same scale as the translational energies [i.e., plotted using the fraction of the ions' translational energy converted into internal energy as a scaling factor (Ref. 31)]. (a) shows the result for an internal energy distribution with a single component halfway between the distributions for the solidlike and liquidlike clusters; (b) shows the result for a filled-in bimodal energy distribution; (c) shows the result for a partially filled-in bimodal energy distribution; and (d) shows the result for the calculated bimodal energy distribution from Fig. 5.

and the cluster on each collision. Under these circumstances, the energy added or removed from a cluster in a collision with a buffer gas atom is

$$E_{\text{rem}} = k_B(T_{\text{cluster}} - T_{\text{buffer}}), \quad (5)$$

where  $k_B$  is the Boltzmann constant and  $T_{\text{cluster}}$  and  $T_{\text{buffer}}$  are the temperatures of the cluster and the buffer gas, respectively. The cooling or heating rate depends on the number of vibrational degrees of freedom in the cluster and the collision rate. With our experimental conditions, we estimate from the collision rate and Eq. (5) that it takes around a 1–2  $\mu\text{s}$  to equilibrate the internal energies of the clusters studied here. This means that the melting and freezing rates (at the melting temperature) must be less than around  $10^6 \text{ s}^{-1}$  in order for the bimodal internal energy distribution to be established.

In order to test the sensitivity of the simulated peak shape to the internal energy distribution, simulations were performed at 640 K with a number of different distributions. Figure 6(a) shows the result for an internal energy distribution with a single component halfway between the liquidlike and solidlike distributions (the dashed line in the figure shows the distribution). A single narrow component in the internal energy distribution is expected if the time between melting and freezing transitions is much shorter than the time required for equilibration of the internal energy distribution, or if there is static phase coexistence with synchronized melting. Synchronized melting will occur in our experiments if the time it takes for the clusters to melt is comparable to the experimental time scale (in this case, the transit time through the temperature variable extension, which is 1–2 ms).<sup>34</sup> The smooth green line in Fig. 6(a) is the result of the simulation described above and the blue lines (with fluctua-

tions) are the experimental results. This internal energy distribution clearly provides a poor fit to the measurements. For Fig. 6(a) we used an internal energy distribution with the same width as a single component (i.e., for the all liquid or all solid states). This is the lower limit for the width in the transition region.<sup>35</sup> For Fig. 6(b) we used an internal energy distribution with the region between the two peaks filled in. This type of distribution might occur in the transition region between dynamic and static phase coexistence with synchronized melting, for static phase coexistence with unsynchronized melting, or when the time between melting and freezing transitions is comparable with the time required for energy equilibration. While the agreement with the measured peak is still not good, it is a marked improvement over that in Fig. 6(a).

Figure 6(c) shows the result for a partially filled-in bimodal distribution and Fig. 6(d) reproduces the result for the calculated bimodal distribution from Fig. 5. This distribution clearly provides the best fit to the experimental results, though the partially filled-in bimodal distribution in Fig. 6(c) is a close second.

## V. A SIMPLER PROBE OF PHASE COEXISTENCE

It is a lot of work to measure the fraction that dissociates over its full range (i.e., from 0 to 1), so here we develop a probe of the internal energy distribution that is less time consuming and hence more readily applicable to a broad range of cluster sizes. The method is based on determining the derivative of the fraction dissociated with respect to the translational energy at 50% dissociation. Around 20 mass spectra are measured at translational energies that lead to around 30%–70% dissociation and then the fractions that dissociate are fit to an S-shaped function  $f = 1/(1 + \exp((E_T - E_T^{50})/s))$ , where  $E_T$  is the translational energy,  $E_T^{50}$  is the translational energy where  $f = 0.5$  (50% dissociation), and  $s$  is a parameter that describes the slope.  $E_T^{50}$  and  $s$  are fit to the data using a least-squares procedure. The slope at  $E_T^{50}$  is  $1/(4s)$ .

Figure 7 shows the derivatives at 50% dissociation plotted against temperature for  $\text{Al}_{100}^+$ ,  $\text{Al}_{101}^+$ ,  $\text{Al}_{126}^+$ , and  $\text{Al}_{127}^+$ . A bimodal internal energy distribution at the center of the melting transition will lead to a minimum in the derivative. The solid black points are the measured derivatives (the average of two or three independent measurements). The solid red line shows derivatives obtained from the simulations described in the preceding section which use internal energy distributions calculated assuming dynamic phase coexistence [Eq. (4)]. We adjust the width of the Gaussian to fit the points away from the minimum and then see if the model reproduces the minimum. The unfilled red squares show the calculated derivatives at the center of the melting transitions. The unfilled green triangles show the values at the center of the melting transitions for an internal energy distribution with a single narrow component, part (a) in Fig. 6; the unfilled green diamonds show the values for the filled-in bimodal distribution, part (b) in Fig. 6; and the unfilled green circles show the values for the partially filled-in distribution shown in part (c) of Fig. 6.

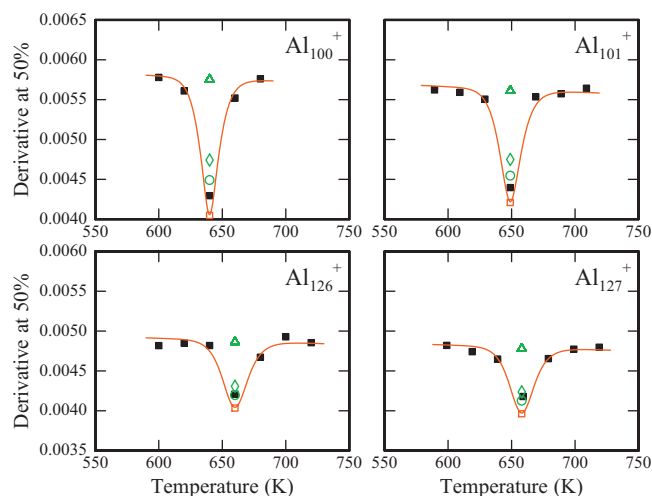


FIG. 7. (Color) The derivative of the fraction dissociated at 50% dissociation plotted against temperature for  $\text{Al}_{100}^+$ ,  $\text{Al}_{101}^+$ ,  $\text{Al}_{126}^+$ , and  $\text{Al}_{127}^+$ . The derivative should show a minimum at the melting transition for a bimodal internal energy distribution. The solid black points are the measured derivatives (the average of two or three independent measurements). The solid red line shows results of simulations described in the text with energy distributions calculated assuming dynamic phase coexistence [Eq. (4)]. The unfilled red squares show the values at the center of the melting transitions. The unfilled green triangles show the values at the center of the melting transitions for the internal energy distribution with a single narrow component, part (a) in Fig. 6; the unfilled green diamond show the values for the filled-in bimodal distribution in part (b) in Fig. 6; and the unfilled green circles show the values for the partially filled-in distribution shown in part (c) of Fig. 6.

The model does a good job of reproducing the minimum for  $\text{Al}_{100}^+$ , in agreement with what was found above (see Fig. 6). The agreement for  $\text{Al}_{101}^+$  is also good. In both cases the minimum in the simulations is slightly deeper than in the measurements.

For  $\text{Al}_{126}^+$  and  $\text{Al}_{127}^+$  the agreement is slightly poorer than for the smaller clusters, and more consistent with a partially filled-in bimodal distribution like that shown in part (c) of Fig. 6. The partial filling in of the bimodal energy distribution could result from the time between melting and freezing transitions becoming comparable to the time required for equilibration of the internal energy distribution. On the other hand, the filling in could indicate the beginning of the transition to static phase coexistence. If the clusters behaved like a macroscopic object and displayed a static phase coexistence, there would not be a minimum in the internal energy distributions. Hence, the change from dynamic to static phase coexistence, which must occur with increasing cluster size, will be signaled by the disappearance of the minimum in the derivatives at the center of the melting transition. This change may occur abruptly over a narrow range of cluster sizes, or gradually over a wider range. In the later case, the minimum will gradually become less deep. The change may well be nonmonotonic, the structure, for example, may influence the transition.

For all clusters in Fig. 7, the differences predicted for the different internal energy distributions are not very large. This is because of the broadening that results from the distribution of energies transferred in the multicollision excitation process and from the slow increase in the fraction of clusters that dissociate on the experimental time scale as the total

internal energy is increased. The differences are largest for  $\text{Al}_{100}^+$  and smallest for  $\text{Al}_{126}^+$  and  $\text{Al}_{127}^+$  (which are very similar) and they are correlated with the latent heat per atom. It follows that our ability to distinguish between the different internal energy distributions will improve as the latent heat per atom becomes larger. Even for  $\text{Al}_{100}^+$ , the latent heat per atom is still only slightly larger than half of the bulk value, and so the situation should improve for larger cluster sizes.

## VI. CONCLUSIONS

We have used multicollision induced dissociation to probe the internal energy distributions of melting aluminum clusters. The results can be fit with a model where the distributions become bimodal at the center of the melting transition with a low energy component due to entirely solidlike clusters and a high energy component due to entirely liquidlike. This indicates that the clusters display dynamic phase coexistence and shows that at least for  $\text{Al}_{100}^+$  and  $\text{Al}_{101}^+$  the time between melting and freezing transitions is larger than the time required for energy equilibration (which is estimated to be around 1–2  $\mu\text{s}$  under our conditions). For  $\text{Al}_{126}^+$  and  $\text{Al}_{127}^+$ , it appears that the bimodal distributions are partially filled in. This indicates that either the clusters are beginning to shift to static phase coexistence or that the time between melting and freezing transitions has become comparable to the time for energy equilibration.

## ACKNOWLEDGMENTS

We gratefully acknowledge the support of the National Science Foundation.

- <sup>1</sup>C. L. Briant and J. J. Burton, *J. Chem. Phys.* **63**, 2045 (1975).
- <sup>2</sup>R. S. Berry, J. Jelinek, and G. Natanson, *Phys. Rev. A* **30**, 919 (1984).
- <sup>3</sup>T. L. Beck, J. Jelinek, and R. S. Berry, *J. Chem. Phys.* **87**, 545 (1987).
- <sup>4</sup>H. Reiss, P. Mirabel, and R. L. Whetten, *J. Phys. Chem.* **92**, 7241 (1988).
- <sup>5</sup>P. Labastie and R. L. Whetten, *Phys. Rev. Lett.* **65**, 1567 (1990).
- <sup>6</sup>H.-P. Cheng, X. Li, R. L. Whetten, and R. S. Berry, *Phys. Rev. A* **46**, 791 (1992).
- <sup>7</sup>J. P. Rose and R. S. Berry, *J. Chem. Phys.* **98**, 3246 (1993).
- <sup>8</sup>B. Vekhter and R. S. Berry, *J. Chem. Phys.* **106**, 6456 (1997).
- <sup>9</sup>Consider a solid macroscopic object at its melting temperature. Its internal energy corresponds to the energy of the solid, and the energy distribution is narrow. If heat is transferred to the object, its internal energy increases and some of the solid melts. As more heat is transferred, more solid melts and the internal energy of the system (solid plus liquid) shifts to higher values until eventually the entire solid melts. The width of the internal energy distribution during this melting transition is the thermal width of the solid and liquid components, plus a contribution from fluctuations in the amounts of solid and liquid (which is small for a macroscopic object, but will become substantial for a small cluster).
- <sup>10</sup>J. Luo, U. Landman, and J. Jortner, in *Physics and Chemistry of Small Clusters*, NATO Advanced Studies Institute, Series B Vol. 158, edited by P. Jena, B. K. Rao, and S. Khanna (Plenum, New York, 1987), p. 155.
- <sup>11</sup>C. L. Cleveland, U. Landman, and W. D. Luedtke, *J. Phys. Chem.* **98**, 6272 (1994).
- <sup>12</sup>C. L. Cleveland, W. D. Luedtke, and U. Landman, *Phys. Rev. B* **60**, 5065 (1999).
- <sup>13</sup>S. C. Hendy, *Phys. Rev. B* **71**, 115404 (2005).
- <sup>14</sup>D. Schebarchov and S. C. Hendy, *J. Chem. Phys.* **123**, 104701 (2005).
- <sup>15</sup>D. Schebarchov and S. C. Hendy, *Phys. Rev. Lett.* **95**, 116101 (2005).
- <sup>16</sup>D. Schebarchov and S. C. Hendy, *Phys. Rev. Lett.* **96**, 256101 (2006).
- <sup>17</sup>M. Schmidt, R. Kusche, W. Kronmüller, B. von Issendorf, and H. Haberland, *Phys. Rev. Lett.* **79**, 99 (1997).
- <sup>18</sup>M. Schmidt, R. Kusche, B. von Issendorf, and H. Haberland, *Nature (London)* **393**, 238 (1998).

- <sup>19</sup>M. Schmidt and H. Haberland, *C. R. Phys.* **3**, 327 (2002).
- <sup>20</sup>M. Schmidt, J. Donges, Th. Hippler, and H. Haberland, *Phys. Rev. Lett.* **90**, 103401 (2003).
- <sup>21</sup>A. A. Shvartsburg and M. F. Jarrold, *Phys. Rev. Lett.* **85**, 2530 (2000).
- <sup>22</sup>G. A. Breaux, R. C. Benirschke, T. Sugai, B. S. Kinnear, and M. F. Jarrold, *Phys. Rev. Lett.* **91**, 215508 (2003).
- <sup>23</sup>G. A. Breaux, D. A. Hillman, C. M. Neal, R. C. Benirschke, and M. F. Jarrold, *J. Am. Chem. Soc.* **126**, 8628 (2004).
- <sup>24</sup>G. A. Breaux, B. Cao, and M. F. Jarrold, *J. Phys. Chem. B* **109**, 16575 (2005).
- <sup>25</sup>J. Bösiger and S. Leutwyler, *Phys. Rev. Lett.* **59**, 1895 (1987).
- <sup>26</sup>M. Y. Hahn and R. L. Whetten, *Phys. Rev. Lett.* **61**, 1190 (1988).
- <sup>27</sup>M. Schmidt, R. Kusche, T. Hippler, J. Donges, W. Kronmüller, B. von Issendorff, and H. Haberland, *Phys. Rev. Lett.* **86**, 1191 (2001).
- <sup>28</sup>C. M. Neal, A. K. Starace, and M. F. Jarrold, *Phys. Rev. B* **76**, 054113 (2007).
- <sup>29</sup>C. M. Neal, A. K. Starace, and M. F. Jarrold, *J. Am. Soc. Mass Spectrom.* **18**, 74 (2007).
- <sup>30</sup>C. M. Neal, G. A. Breaux, B. Cao, A. K. Starace, and M. F. Jarrold, *Rev. Sci. Instrum.* **78**, 075108 (2007).
- <sup>31</sup>M. F. Jarrold and E. C. Honea, *J. Phys. Chem.* **95**, 9181 (1991).
- <sup>32</sup>D. Poland, *J. Chem. Phys.* **126**, 054507 (2007).
- <sup>33</sup>M. F. Jarrold and E. C. Honea, *J. Am. Chem. Soc.* **114**, 459 (1992).
- <sup>34</sup>This behavior might occur, for example, for large clusters, where the time it takes to heat them is comparable to the transit time through the temperature variable extension.
- <sup>35</sup>It does not include a contribution from fluctuations in the amounts of solid and liquid.